ACS APPLIED MATERIALS & INTERFACES

www.acsami.org

Research Article

# Molybdenum Trioxide Nanocubes Aligned on a Graphene Oxide Substrate for the Detection of Norovirus by Surface-Enhanced Raman Scattering

Ojodomo J. Achadu, Fuyuki Abe, Tetsuro Suzuki, and Enoch Y. Park*

Cite This: https://dx.doi.org/10.1021/acsami.0c14729

Read Online

ACCESS | Metrics & More | Article Recommendations | Supporting Information

**ABSTRACT:** A novel biosensing system based on graphene-mediated surface-enhanced Raman scattering (G-SERS) using plasmonic/magnetic molybdenum trioxide nanocubes (mag-$MoO_3$ NCs) has been designed to detect norovirus (NoV) via a dual SERS nanotag/substrate platform. A novel magnetic derivative of $MoO_3$ NCs served as the SERS nanotag and the immunomagnetic separation material of the biosensor. Single-layer graphene oxide (SLGO) was adopted as the 2D SERS substrate/capture platform and acted as the signal reporter, with the ability to accommodate an additional Raman molecule as a coreporter. The developed SERS-based immunoassay achieved a signal amplification of up to ~$10^9$-fold resulting from the combined electromagnetic and chemical mechanisms of the dual SERS nanotag/substrate system. The developed biosensor was employed for the detection of NoV in human fecal samples collected from infected patients by capturing the virus with the aid of NoV-specific antibody-functionalized magnetic $MoO_3$ NCs. This approach enabled rapid signal amplification for NoV detection with this biosensing technology. The biosensor was tested and optimized using NoV-like particles within a broad linear range from 10 fg/mL to 100 ng/mL and a limit of detection (LOD) of ~5.2 fg/mL. The practical applicability of the developed biosensor to detect clinical NoV subtypes in human fecal samples was demonstrated by effective detection with an LOD of ~60 RNA copies/mL, which is ~$10^3$-fold lower than that of a commercial enzyme-linked immunosorbent assay kit for NoV.

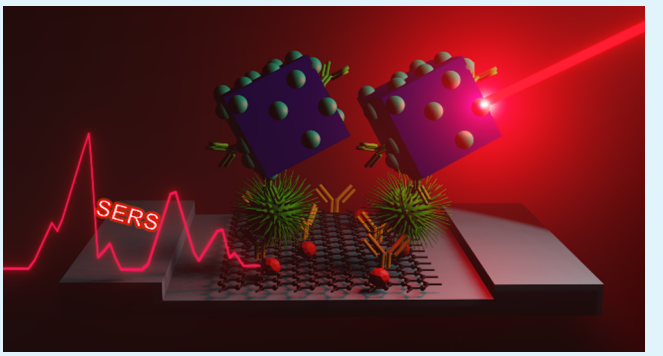


**KEYWORDS:** *molybdenum nanocubes, single-layer graphene oxide, dual SERS nanotag/substrate, SERS-based immunoassay, norovirus, immunomagnetic separation*



## 1. INTRODUCTION

Norovirus (NoV), the leading cause of gastritis and colitis (acute gastroenteritis),[1,2] is typically detected using a real-time reverse transcription-polymerase chain reaction (RT-qPCR) technique as the current gold standard.[3] However, enzyme-linked immunosorbent assay (ELISA) and immunochromatography are also used because of their convenience.[3,4] NoV detection in clinical fecal samples remains a challenge using these techniques. Therefore, immunomagnetic separation protocols combined with highly sensitive detection platforms such as surface-enhanced Raman scattering (SERS) spectroscopy have emerged as potential biosensing platforms.[5] The reason is that the SERS technique greatly benefits from advances in nanofabrication, as demonstrated by the use of various nanostructures and design strategies for SERS-based detection of pathogenic agents. For instance, SERS nanotags consisting of $Fe_3O_4$@Ag hybrid nanoparticles (NPs) were used for the simultaneous detection of influenza A/H1N1 virus and human adenovirus.[6] A SERS-based magnetic multimodal imaging and detection system for the cancer biomarker $CD_{19}$(+) B lymphoblast was reported using hollow gold–silver nanospheres.[7] A plasmonic Au–Ag-coated GaN substrate was reportedly employed for hepatitis B virus antigen detection from human blood via a microfluidic SERS system.[8] Ag nanoislands and nanoflowers on chitin nanopillars have been used to generate SERS "hotspots" for animal virus detection.[9] Thus, SERS-based detection technology is constantly evolving to develop high-level immunoassays for clinical diagnostics.

Generally, SERS-based sandwich or competitive immunoassays invariably entail the use of single-component SERS nanotags on bare glass slides as capture platforms.[10,11] Sample pretreatment or isolation of antigens from sample matrices is vital in immunoassays. The tendency of clinical samples to

Received: August 16, 2020
Accepted: September 10, 2020

present high-complexity matrices, thereby necessitating decreased detection sensitivities, makes this issue more difficult.[8] In another scenario, SERS nanotags can easily exhibit unstable signals due to aggregation and/or desorption of Raman reporters conjugated on the surface of metal nanostructures.[12,13] The analytical sensitivity, reproducibility, and overall reliability of such biosensors can be seriously undermined by these issues. Thus, nanotags have been embedded in protective shells such as silica or polymers to preserve their integrity, reduce aggregation, and guarantee stability even in high ionic strength solutions.[12,14−16] For cell imaging and immunoassays, this strategy also provides biocompatibility.[12] However, the broad dimensions and vulnerabilities of encapsulating shells and the possibility of signal interference limit their convenient use.[12,17,18]

To address these problems, in this work, emerging SERS "hotspot" engineering concepts[19] were adopted using a novel dual nanotag/substrate system for the developed SERS-based immunoassay technology. New plasmonic-/magnetic-derivatized $MoO_3$ nanocubes (mag-$MoO_3$ NCs) and a single-layer graphene oxide (SLGO)-based solid capture platform were used as the dual SERS nanotag and substrate, respectively. This technology has been proposed for a number of reasons. First, SERS signal amplification can be achieved by synergizing the Raman signal enhancement properties of plasmonic $MoO_3$ NCs via an electromagnetic mechanism. This feature can be coupled with the excellent chemical mechanism-based SERS enhancement properties of the large nanosheets of SLGO to attain engineered wide-area "hotspots" in a sensitive graphene-mediated SERS (G-SERS) immunoassay.[19−22] Second, the combination of the dual SERS nanotag/substrate herein offers several all-in-one advantages. For example, the magneto-plasmonic $MoO_3$ NCs can simultaneously deliver plasmonic SERS enhancement and immunomagnetic separation of the target virus, which is best suited for the assay of real/clinical samples containing high-solid matrices.[23] Moreover, the SLGO platform was adapted because of its dual functionality as a Raman reporter/SERS enhancement substrate. Consequently, this biosensor does not necessarily need an additional Raman molecule as a signal reporter. SLGO is an indispensable additive and building block for the developed SERS-based immunoassay platform on a flat surface, enabling the immunoassay to be performed on a solid platform with considerable simplicity. In addition, the presence of rich functional groups and high electron mobility on the surface of the large planar nanosheets of SLGO[20] enable the easy conjugation of the capture antibodies and a classical Raman reporter as an additional signal reporter (not necessary but used to probe the extent of the analytical sensitivity limit of the developed biosensor). Lastly, SLGO may also quench the background fluorescence resulting from residual sample matrices or reporter molecules,[20,21] an additional benefit for its use as a SERS substrate.

Therefore, in this research, the SERS and optical features of the dual SERS nanotag/substrate were combined to design a highly scalable platform for ultrasensitive and selective detection of NoV via SERS signal amplification. NoV in human fecal samples was captured using mag-$MoO_3$ NCs and magnetically separated from the sample matrices. The formed NoV/mag-$MoO_3$ NC immunocomplex was deposited on the SLGO capture substrate under magnetic influence for the SERS immunoassay. The target NoV-like particles (NoV-LPs)/NoV was tethered between the antibody-mag-$MoO_3$ NCs and the SLGO-antibody (or SLGO-4MBA-antibody) capture platforms to form a sandwich-type immunocomplex loop. NoV-LPs were assayed in human serum as a detection medium, and a remarkable limit of detection (LOD) of 9.5 fg/mL was obtained. The clinical application of the developed biosensor was further tested with human fecal samples, and an excellent LOD of ∼60 copies/mL was achieved with minimal inhibitory matrix effects. Overall, it is envisaged that the developed SERS-based immunoassay system can be adopted for point-of-care (POC) testing in clinical and diagnostic practice.

## 2. EXPERIMENTAL SECTION

**2.1. Materials.** Ammonium molybdate tetrahydrate, polyvinylpyrrolidone (PVP), and hydrogen peroxide (30%) were supplied by FUJIFILM Wako Pure Chemical Corporation (Osaka, Japan). Glutaraldehyde, iron(III)chloride, bovine serum albumin (BSA), *N*-hydroxysuccinimide (NHS), *N*-(3-dimethylaminopropyl)-*N*′-ethylcarbodiimide hydrochloride (EDC), and human serum (from human male AB plasma, USA origin, sterile-filtered) were purchased from Sigma-Aldrich (St. Louis, Missouri, USA). 4-Mercaptobenzoic acid (4-MBA) and *N*-(2-aminoethyl)maleimide hydrochloride were supplied by Tokyo Chemical Industries (Tokyo, Japan). SLGO flakes were obtained from ACS Material, LLC (Pasadena, California, USA). All experiments and solution preparations were carried out using ultrapure doubly distilled deionized (DI) water (>18 MΩ·cm) except where otherwise specified.

**2.2. Instrumentation.** SERS measurements/confocal Raman spectroscopy were performed on an NRS-7100 on-board microscopic laser Raman spectrophotometer (JASCO, Tokyo, Japan) using a 785 nm laser. The Raman peak of a silicon reference standard at 520 $cm^{-1}$ was used for calibration. The measurements were performed using a 100× objective lens at 1% laser power and 2 s integration time. The acquired SERS spectra baselines were removed using f500 spectrograph software (JASCO). The individual SERS spectrum acquired and shown in the data figures is an average of 10 replicated measurements, except where otherwise specified. Multipoint analysis was performed by the high-speed mapping function from a 50 $\mu$m × 50 $\mu$m area with a step size of 2 $\mu$m and an exposure time of 2 s. The laser power was 1%, and the time of acquisition was set to 1 s at each pixel.

X-ray photoelectron spectroscopy (XPS) was performed on an ESCA1600 system (ULVAC-PHI Inc., Tokyo, Japan) with an Al K$\alpha$ X-ray source (1486.6 eV) and a hemispherical electron analyzer. Ground-state electronic absorption (UV/vis) spectra were recorded on a filter-based multimode microplate reader (Infinite F200 M; Tecan, Ltd., Männedorf, Switzerland). Field emission-scanning transmission electron microscopy (FE-STEM) with energy-dispersive X-ray spectroscopy (EDS) analysis was performed using a JEM-2100F field emission scanning electron microscope (JEOL, Ltd., Tokyo, Japan) operating at 200 kV. TEM images were obtained using a JEM-2100F system (JEOL, Ltd., Tokyo, Japan) operating at 100 kV. Dynamic light scattering (DLS) analysis was performed using a Malvern Zetasizer Nano series Nano-ZS90 system (Malvern Instruments Ltd., Malvern, UK). Powder X-ray diffraction (PXRD) analysis was performed using a RINT ULTIMA XRD system (Rigaku Co., Tokyo, Japan) with a Ni filter and a Cu K$\alpha$ source. Data were collected over $2\theta$ = 10−90° at a scan rate of 0.01°/step and 10 s/point. Fourier-transform infrared (FTIR) spectroscopy was performed using an FT/IR-6300 spectrometer with an ATR PRO610P-S (JASCO).

**2.3. Biological Materials.** Monoclonal antibodies (NS14, isotype-IgG acquired from the spleen cells of orally immunized mice), which are specific and broadly reactive to genogroup II of NoV,[24] were used in this work for the sandwich-type immunoassay. Following the standard protocol for virus-like particle preparation,[25] GII.4 NoV-LPs were expressed in *Trichoplusia ni* BTL-Tn 5B1-4 (Tn5) by transfection of recombinant baculovirus TCN-VP1


https://dx.doi.org/10.1021/acsami.0c14729
ACS Appl. Mater. Interfaces XXXX, XXX, XXX−XXX

(Invitrogen, San Diego, CA, USA), which is purified, quantified, and used to test, optimize, and implement the immunoassay platform for detection. Clinical fecal samples of gastroenteritis-infected patients were collected, as defined by the statutory and regulatory protocol. To do so, ~1.0 mg of the solid fecal sample was added to a minimum of 9 μL of phosphate-buffered saline (PBS, pH 7.4); the obtained supernatant separated from the solid portion was used as the detection sample. The NoV sampling protocol was carried out according to the guidelines of the Ethics Committee of the Environment and Hygiene Institute in Shizuoka Prefecture (September 14, 2016). Influenza virus A/New Caledonia (20/99/IVR/116) (H1N1) was purchased from ProSpec-Tany TechnoGene Ltd. (Rehovot, Israel). Clinically isolated influenza virus A/Yokohama/110/2009 (H3N2) was kindly provided by Dr. C. Kawakami of Yokohama City Institute of Health, Japan. Goat antirabbit IgG-HRP was purchased from Santa Cruz Biotechnology (Dallas, Texas, USA). Zika virus was kindly provided by Prof. K. Morita of the Institute of Tropical Medicine, Nagasaki University. HEV-LPs were prepared as previously reported.[26] Dengue virus cDNA was synthesized by Integrated DNA Technologies (Coralville, Iowa, USA). In this study, the sensitivity of the developed biosensor for NoV detection was compared with that of two rapid test kits based on ELISA and paper-based lateral flow techniques. The commercial ELISA kit for NoV detection—*NV EIA "Seiken"*—was supplied by Denka Co., Ltd., Tokyo, Japan. The paper-based lateral flow NoV antigen kit for rapid testing was supplied by Sekisui Medical Co., Ltd., Japan.

**2.4. Synthesis of Mag-$MoO_3$ NCs and Antibody Conjugation.** A mixture of 8.0 mL of 30% $H_2O_2$ and 5.0 mL of deionized water was added to 100 mg (0.08 mmol) of ammonium molybdate tetrahydrate and stirred for 1 h. Then, 2.0 mL of 0.1 M NaOH was added to the resulting mixture, and the excess $H_2O_2$ was expelled by heating at 70 °C for 30 min until the bubbling stopped. To 5.0 mL of the resulting mixture were added 0.01 mg of PVP and 2.5 mg (0.015 mmol) of $FeCl_3{\cdot}6H_2O$ in 5 mL of ammonia solution. The product was sonicated for 2 h, transferred to a Teflon-lined stainless-steel autoclave, and heated at 200 °C for 18 h. Afterward, the product was washed three times with a mixture of ethanol/acetone by centrifugation to remove excess PVP, further purified using an external magnetic separation approach and dried under vacuum at 60 °C. Furthermore, the mag-$MoO_3$ NCs were surface-functionalized with carboxylic groups for antibody conjugation by incubating with 2.0 mL of glutaraldehyde in ethanol and mechanically stirred for 12 h at room temperature. The product was purified by magnetic separation and centrifugation.

To further conjugate the anti-NoV antibody (NS14) to the mag-$MoO_3$ NCs, EDC (100 μL, 0.1 M) was stirred with 5 mL of mag-$MoO_3$ NCs for 30 min to activate its carboxylic group. Then, 100 μL (0.1 M) of NHS was added to the mixture, followed by the addition of 10.1 μg/mL anti-NoV antibody (NS14) in PBS (pH 7.6) and mechanically stirred at 7 °C overnight. The obtained Ab-conjugated mag-$MoO_3$ NCs were washed and magnetically separated to remove unbound antibodies, followed by incubation with 5% BSA to minimize nonspecific interactions. Then, the excess BSA was removed by centrifugation (3000*g*, 5 min), and the conjugate was redissolved in ultrapure DI water for further use or stock in a refrigerator when not used immediately. The conjugation of the anti-NoV antibody to mag-$MoO_3$ NCs was confirmed by ELISA using a microplate reader (model 680; Bio-Rad, Hercules, California, USA). The amount of NoV antibodies bound to the mag-$MoO_3$ NCs was estimated by a ninhydrin-based protein assay. Details are given in the Supporting Information.

**2.5. Capture Platform/Substrate Preparation.** *2.5.1. SLGO-Antibody Substrate.* The SLGO solid platform substrate was prepared by drop-casting and immobilization of SLGO on prepared glass slides.[27] Briefly, μ-quartz glass slides (3 mm thick, 8-well square cavity) were soaked in 10 mL of acid piranha solution ($H_2SO_4/H_2O_2$ [30%] at the ratio of 3:1), followed by rinsing with copious amounts of deionized water and then ethanol. Each cavity of the glass slide was blown to dryness using a stream of $N_2$ gas, and then, each slide was placed in a vacuum oven for 4 h at 70 °C. After this time, an aqueous solution of SLGO was deposited on the oven-dried quartz slides, which were further placed in a vacuum oven at 70 °C for 8 h to obtain the SLGO coating, followed by conjugation of the anti-NoV antibody using EDC/NHS chemistry. The carboxylic acid groups on the SLGO were activated by immersing the SLGO-coated glass slide in a mixture of EDC (100 μL, 0.1 M) and NHS (100 μL, 0.1 M) with continuous stirring for 4 h in PBS (pH 7.6). Then, 250 μg/mL anti-NoV antibody (NS14) was added to the SLGO-coated glass slide-submerged mixture and incubated for 8 h at 7 °C. Finally, the antibody-functionalized SLGO (SLGO-antibody) capture substrate was thoroughly rinsed with DI water and PBS (pH 7.6) several times to remove attached/excess molecules and antibodies. To block the nonspecific binding sites on the substrate, the glass slides were incubated in 5% BSA in PBS for 1 h. The prepared capture substrates were stored at 4 °C before SERS measurements.

*2.5.2. SLGO-4MBA-Antibody Substrate (Dual Reporter System).* The preparation steps for the SLGO-4MBA-antibody capture substrate (dual reporter system) are shown in Figure S1 of the Supporting Information. The covalent conjugation of 4-MBA to the SLGO substrate was achieved via a two-step process using a maleimide linker (*N*-(2-aminoethyl)maleimide) with terminal amine ($NH_2$) and maleimide moieties. Detailed procedures for SLGO-4MBA capture substrate preparation and anti-NoV antibody conjugation are provided in S1 and Figure S1 of the Supporting Information.

**2.6. Immunoassay Protocol.** *2.6.1. Immunoassay of NoV-LPs in PBS/Human Serum.* The immunoassay of NoV-LPs was carried out separately in PBS (pH 7.6) and human serum media. In PBS medium, different concentrations of NoV-LPs (1.0−$10^7$ fg/mL) were sequentially added to the SLGO-antibody or SLGO-4MBA-antibody capture substrates and allowed to incubate for 15 min. Then, under the influence of an exterior magnet, 200 μL (2 mg/mL) of the antibody-mag-$MoO_3$ NCs was added to the NoV-LP-captured SLGO-based substrates, allowing another 15 min for sandwich immunocomplex formation. The resultant immunocomplex formed on the substrates was washed with ultrapure DI water and PBS to remove the unbound virus and other matrices.

To detect NoV-LPs in human serum, the above-described procedure was changed slightly. Direct capture on the SLGO-antibody capture substrates was replaced by initially capturing NoV-LPs and magnetically separating/enriching them from the human serum medium using antibody-mag-$MoO_3$ NCs. To do so, NoV-LPs (1.0 to $10^7$ fg/mL in 50% human serum) were separately incubated for 15 min with 200 μL (2 mg/mL) of the antibody-mag-$MoO_3$ NCs in microcentrifuge tubes. The mixture was centrifuged and magnetically separated to collect the NoV-LP-enriched immunocomplex. The immunocomplex was further redissolved in PBS (pH 7.6) and then deposited on the SLGO-based capture platform. Finally, the substrates were air-dried, and the SERS measurements were recorded under a magnetic field. The capture platform/mag-$MoO_3$ NCs without the anti-NoV antibodies were used as controls. BSA binding on the antibody-conjugated capture substrate/mag-$MoO_3$ NCs instead of the NoV-LPs was used as the negative control. The noncoated and SGLO-coated zones on the glass slides were also used as controls for SERS multipoint mapping. All the controls were treated under similar conditions with the developed immunoassay protocol. The details are provided in the Supporting Information, S5.

*2.6.2. Immunoassay of NoV in Human Fecal Clinical Samples.* The clinical samples were analyzed by deploying an immunomagnetic separation protocol. Real-time RT-PCR determined the NoV concentration of fecal samples (GII.2: $6.2 \times 10^7$ RNA copies/mL, GII.3: $7.2 \times 10^8$ RNA copies/mL, and GII.4: $5.7 \times 10^7$ RNA copies/mL). In this case, the detection performance was evaluated, ranging from 100 RNA copies/mL to $10^7$ RNA copies/mL NoV. Thus, NoV (10 to $10^6$ RNA copies/mL) was separately incubated with 200 μL (2 mg/mL) of the antibody-mag-$MoO_3$ NCs in a microcentrifuge tube for 15 min for the immunoreaction between antibody-mag-$MoO_3$ NCs and NoV. The immunocomplex containing NoV/antibody-mag-$MoO_3$ NCs was washed with PBS repeatedly and collected separately using a magnet. The resulting NoV-captured antibody-mag-$MoO_3$


https://dx.doi.org/10.1021/acsami.0c14729
ACS Appl. Mater. Interfaces XXXX, XXX, XXX−XXX

NC complex was further redispersed in PBS (pH 7.6) and deposited on the SLGO-based capture platforms to obtain the sandwich immunocomplex between the virus and the antibody for SERS measurements. Following our proposed system, the clinical NoV was also tested and compared using a commercial ELISA kit (NV-EIA) and a paper-based lateral flow rapid test kit for NoV detection.

## 3. RESULTS AND DISCUSSION

**3.1. Design/Working Principle.** New analytical SERS systems are emerging based on "hotspot" engineering principles.[19] The concept is to synergize the traditional metal-based SERS system with functional materials, including graphene nanostructures, semiconductor materials ($TiO_2$), and piezoelectric polymers, to provide improved electromagnetic and chemical properties in hybrid SERS platforms.[19] Through engineered "hotspots," SERS sensitivities have been greatly increased to thresholds that could not be attained by plasmonic nanostructures alone, such as single-molecule detection using G-SERS.[19,20] Accordingly, SERS-based biosensors have been designed using plasmonic nanostructures (0D/1D) and multidimensional (2D/3D) platforms to exploit the electromagnetic and chemical mechanisms of Raman signal enhancements of neighboring molecules.[19,28] In addition, SERS-based immunoassays are usually focused on complex immunoreactions between target antigens and complementary SERS nanotags and/or substrates.[8]

The concepts mentioned above have been used to develop a sensitive SERS-based biosensor for NoV as a target virus in this work. Synergistic coupling interactions between plasmonic mag-$MoO_3$ NCs and chemically active graphene-based substrates (SLGO) are used to induce NoV-LP/NoV-regulated SERS enhancements in this work. The biosensor comprises novel magnetic-derivatized $MoO_3$ NCs (SERS nanotag), SLGO (SERS capture substrate/reporter), anti-NoV antibody (NS14), and 4-MBA (external reporter used to probe the sensitivity limit of the biosensor).[29] The detection principle involves SERS signal amplification implemented by the dual SERS nanotag/substrate (antibody-mag-$MoO_3$ NCs/SLGO-antibody) system as a result of target NoV-LPs/NoV capture in a sandwich immunocomplex. During this process, either the antibody-mag-$MoO_3$ NCs alone or the NoV-captured antibody-mag-$MoO_3$ NCs (which have been magnetically separated from sample matrices) were deposited on the surface of the SLGO-antibody (or SLGO-4MBA-antibody) solid capture platforms to induce enhanced Raman signals of SLGO (or SLGO-4MBA). The developed biosensor benefits from both electromagnetic and chemical-induced coupling interactions around the surface of the dual SERS nanotag/substrate (mag-$MoO_3$ NCs and SLGO system). For real-sample analysis, the magnetic feature of mag-$MoO_3$ NCs was used to isolate/enrich target NoV from human feces with complex matrices.[30,31] Therefore, the biosensor did not require additional magnetic components, thereby simplifying the biosensor's material components. Another advantage of using mag-$MoO_3$ NCs was that the detection system further demonstrated that the SERS measurements under magnetic actuation produced stable and reproducible SERS signal amplification, similar to previous reports.[32,33] The mechanism for this process is not clearly understood. We suspect, however, that the mag-$MoO_3$ NCs may be well-ordered/aligned by the applied magnetic force to create a strong local electric field that can promote the Raman activity of SLGO or SLGO-4MBA to improve the SERS performance of the biosensor.[6,32]

On the other hand, SLGO worked primarily to promote SERS enhancement via a chemical mechanism as a substrate/capture platform.[20,21] SLGO exhibits the characteristic Raman peaks known as the D- and G-bands, which can be used for SERS monitoring without the need for an external Raman reporter molecule.[32] The further advantage of using SLGO as a capture substrate was to ensure that autofluorescence from residual sample matrices was removed.[20] The use of SLGO increased the signal-to-noise ratio of generated SERS signals for the ultrasensitive immunoassay of NoV-LPs or NoV in clinical samples.

**3.2. Dual SERS Nanotag/Substrate "Hotspot" Engineering.** For this particular study, the direct conjugation of 4-MBA, as an additional Raman reporter, to the planar surface of SLGO instead of to the mag-$MoO_3$ NCs was a "hotspot" engineering strategy that requires some discussion. Following experimental observations, it was deduced that the conjugation of 4-MBA to SLGO performed better than conjugation to mag-$MoO_3$ NCs for some obvious reasons. First, unlike the strong thiol selfassembly monolayer usually formed between 4-MBA and Au or Ag NPs,[34] 4-MBA binds weakly to the surface of the mag-$MoO_3$ NCs, generating very weak SERS signals (Figure S3A). This observation was similar to the one observed when 4-MBA was attached to the surface of $SiO_2$-coated Au NPs, producing weak and unclear SERS signals, which then required a layer of Ag NPs to achieve stable and strong SERS signals.[35] In our case, the weak interaction between mag-$MoO_3$ NCs and 4-MBA may be due to the potential electrostatic repulsion between the oxygen-rich surface of the mag-$MoO_3$ NCs and the carboxylic moiety of 4-MBA and/or the desorption of 4-MBA from the surface of the mag-$MoO_3$ NCs. The propensity of Raman reporters to desorb or leach from plasmonic NP surfaces is known to be a major drawback in SERS detection technology.[12,36,37] To address this issue, SERS nanotags are often coated with outer protective layers to avoid leaching of reporter molecules to maintain stable and reproducible SERS signals.[12,13] Therefore, the need to encapsulate mag-$MoO_3$ NCs conjugated with 4-MBA in a protective coating was avoided by conjugating 4-MBA to SLGO instead. This idea was initially thought to be a compromise/trade-off between achieving either more sensitivity or stable and reproducible SERS immunoassays. However, this concern was mitigated by the fact that SLGO, like graphene, is a functional SERS-active 2D nanostructure that enhances the Raman signal of molecules via a chemical mechanism.[38] Hence, the G-SERS approach herein can result in SERS enhancement via $\pi-\pi$ stacking interactions and charge transfer between the SLGO and aromatic 4-MBA molecules.[38,39] In addition, graphene nanostructures are known to be excellent electron transporters, with remarkable electronic conductivity.[20,29] It is then plausible to expect a significant boost in the SERS signals of the SLGO-4MBA system in the presence of plasmonic mag-$MoO_3$ NCs, probably because of a synergistic effect resulting from the interaction between the SLGO-4MBA platform and plasmonic mag-$MoO_3$ NCs. An electronic flow process from the oxygen vacancy-associated electronic states of plasmonic mag-$MoO_3$ NCs[40,41] to the 4-MBA chemisorbed on the SLGO, as the bridge, can drive the SERS enhancements of 4-MBA.[42,43] This effect is similar to that in previous reports, where the Raman signals of 4-MBA-conjugated graphene oxide were significantly enhanced in the presence of the plasmonic semiconductor $TiO_2$.[42,43] In another instance, the chemical properties of $TiO_2$ were


https://dx.doi.org/10.1021/acsami.0c14729
ACS Appl. Mater. Interfaces XXXX, XXX, XXX−XXX

employed to mediate the charge transfer between plasmonic Au or Ag and 4-MBA adsorbed onto $TiO_2$.[44] The rhodamine 6G/graphene platform has also been reported to encounter similar G-SERS enhancement in the presence of Au NPs.[45] A similar phenomenon might have occurred between 4-MBA adsorbed onto SLGO and the plasmonic mag-$MoO_3$ NCs in our biosensing system. A detailed understanding of the actual mechanism occurring herein is beyond the scope of the present work, and it is of interest in the future. Moreover, the large planar surface of SLGO means that many 4-MBA molecules can be accommodated, thereby increasing the chances of interaction with the plasmonic mag-$MoO_3$ NCs. Additionally, the strong covalent bonding and the possibility of $\pi-\pi$ stacking interactions between the aromatic rings of 4-MBA and SLGO can allay concerns regarding the leaching of 4-MBA from the SLGO substrate, unlike mag-$MoO_3$ NCs. Thus, this approach produced stable and reproducible SERS signals required for a robust biosensor. Detailed discussion on the choice of materials used in this work and the evaluation of their SERS properties and various control studies adopted in this work are provided in the Supporting Information (S2−S6; Figures S3−S7, and Table S1).

**3.3. Characterization of Mag-$MoO_3$ NCs and SLGO-Capture Substrate.** A nanocomposite of magnetic-based $MoO_3$ NCs was prepared for the first time by *in situ* grafting of magnetic NPs (MNPs) on the surface of $MoO_3$ NCs. Chemical and/or electrostatic adhesion of the MNPs to the surface of the $MoO_3$ NCs was achieved under hydrothermal conditions (Scheme 1). By controlling the synthetic conditions, cube-shaped mag-$MoO_3$ NCs with good uniformity and excellent optoelectrical/chemical properties were prepared. The shape and size of the mag-$MoO_3$ NCs, as well as the MNP functionalization, were dictated by the hydrothermal temperature and the use of PVP to direct cubic shape formation as a stabilizing agent for the growth of the $MoO_3$ NCs and the reducing agent for MNP formation. A hydrothermal temperature of 200 °C was used to synthesize the composite nanocubes. At temperatures below 200 °C, the composite appeared to be quasispherical in shape (even in the presence of PVP) (Figure S8 in the Supporting Information). This result implies that the synthesis temperature was a critical factor in the achievement of cube-shaped $MoO_3$ NPs. This finding could also mean that the reactivity of PVP and the magnetic precursor changed at 200 °C, with the reduction rate being presumably faster due to higher thermal energy leading to the orderly growth of the magnetic $MoO_3$ NCs.

**Scheme 1. Synthesis of mag-$MoO_3$ NCs; (A) Oxidation of the Mo Precursor Using $H_2O_2$; (B) Hydrothermal Treatment of Oxidized Mo and $FeCl_3$ in the Presence of PVP; (C) Carboxylic Acid Functionalization of the Prepared mag-$MoO_3$ NCs Using Glutaraldehyde; and (D) NoV Antibody Conjugation via EDC/NHS Chemistry**

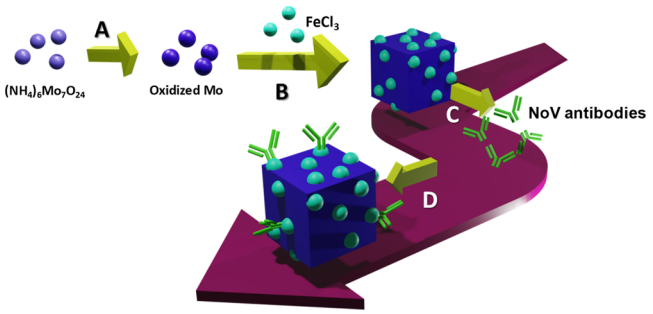


XPS analysis was used to probe the surface chemical and structural compositions of the prepared mag-$MoO_3$ composite nanocubes and their electronic states. The XPS survey spectrum of the nanocubes, with distinct peaks at 235.8 eV (Mo 3d), 285.85 eV (C 1s), 402.5 and 418.3 eV (Mo 3p), 532.4 eV (O 1s), and 710.2 and 718.6 eV (Fe 2p), confirmed the presence of Mo, O, C, and Fe as the principal atoms, as shown in Figure 1a. The high-resolution XPS spectra of the Mo 3d peak (Figure 1b) displayed characteristic deconvoluted strong peaks at 235.42 and 238.57 eV attributed to $Mo^{6+}$, and the peaks at 233.25 eV and 237.05 eV are attributed to the $Mo^{5+}$ state of the $MoO_3$ NCs.[41,46] The deconvoluted O 1s XPS peak (Figure 1c) shows evidence of two species of oxygen-rich moieties on the surface of the mag-$MoO_3$ NCs, likely resulting from Mo and Fe oxides. The grafting of MNPs onto the nanocubes was confirmed by the high-resolution curve-fitted XPS spectrum of Fe 2p, as shown in Figure 1d. The Fe $2p_{1/2}$ peak at 711.1 eV and the Fe $2p_{3/2}$ peak at 724.8 eV correspond to the magnetic component of the cubic nanostructure.

The morphology and size of the prepared mag-$MoO_3$ NCs were adequately examined by TEM (Figure 2a). The mag-$MoO_3$ NCs displayed a well-defined cubic shape with a narrow diameter distribution and edge length/dimension typically within 90−100 nm. Further morphological characterization by FE-STEM revealed the surface grafting of $MoO_3$ NCs with MNPs. Figure 2b presents a typical FE-STEM micrograph of the mag-$MoO_3$ NCs at atomic resolution showing the surface adhesion of MNPs on the cubic-shaped $MoO_3$ NCs (average size of ∼100 nm), with a core-satellite feature, indicating the positive formation of mag-$MoO_3$ NCs. A follow-up DLS/zeta potential measurement was used to assess the hydrodynamic particle size, overall surface charge, and stability of the mag-$MoO_3$ NCs. These experiments probed the size distribution and evaluated the monodispersity/aggregation states of the nanocubes in solution. The average hydrodynamic size diameter of ∼92 ± 3.3 nm and the zeta potential of −42.5 mV (Figure S9 in the Supporting Information) were obtained. The particles were not agglomerated in solution based on the obtained zeta potential value and the average size, which is in close agreement with the TEM results. In addition, the elemental compositional analysis (Figure 3a) and explicit elemental mappings of the prepared nanocubes clearly displayed the presence of Mo as the core component and Fe as the magnetic component (Figure 3b,c). The merged elemental mapping spectra in Figure 3d revealed that the $MoO_3$ NCs have some MNPs scattered around their surface. However, some MNPs can still be visualized as grafted onto the $MoO_3$ NCs. The optical properties of the mag-$MoO_3$ NCs were analyzed by UV−vis spectroscopy to reveal absorption spectra, displaying a deep and strong localized surface plasmonic resonance (LSPR) absorption in the visible region at 738 nm (Figure 4), which is similar to that of other Mo-based nanostructures with tunable optical properties.[41,46,47] This property was utilized for the optical and chemical applications of the prepared mag-$MoO_3$ NCs. To further gain insight into the microstructure of the prepared mag-$MoO_3$ NCs, XRD and Raman measurements were carried out. The XRD pattern depicted in Figure S10A shows diffraction peaks, which indicated the orthorhombic crystal structure of the $MoO_3$ NCs, with well-defined diffraction peaks clearly established according to the (020), (040), (010), and (810)


https://dx.doi.org/10.1021/acsami.0c14729
ACS Appl. Mater. Interfaces XXXX, XXX, XXX−XXX

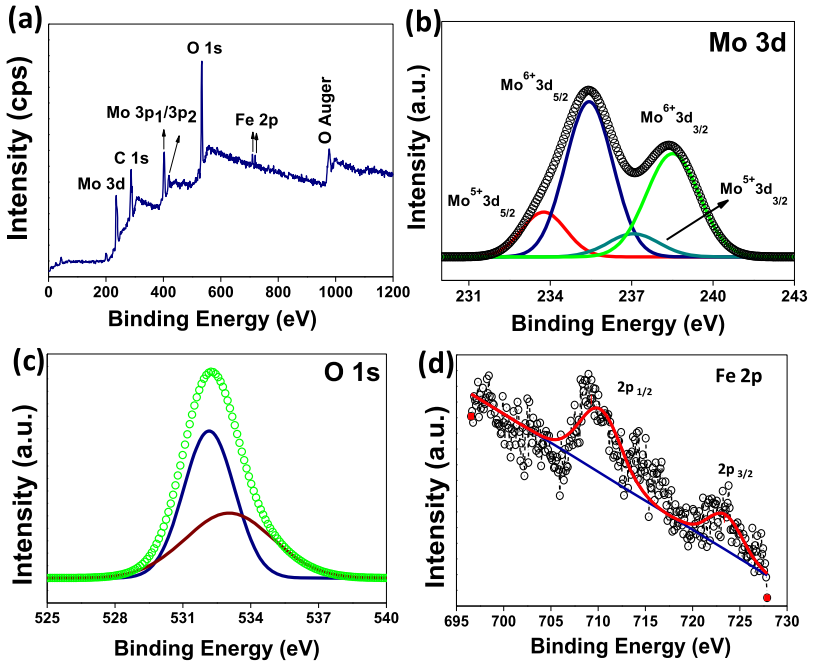


**Figure 1.** XPS characterization data of newly synthesized mag-$MoO_3$ NCs. (a) Wide-scan XPS survey spectra. (b) High-resolution deconvoluted Mo 3d spectra. (c) High-resolution deconvoluted O 1s spectra. (d) High-resolution deconvoluted Fe 2p spectra.

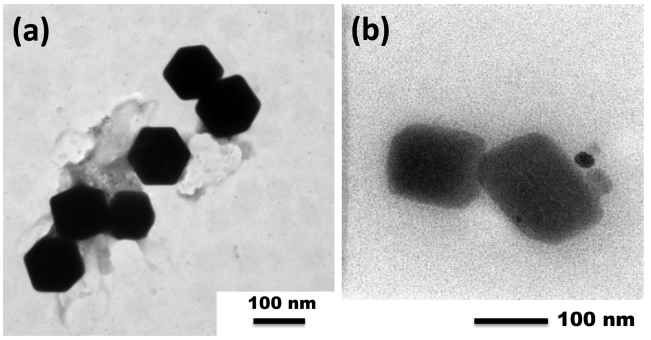


**Figure 2.** Electron microscopy data of mag-$MoO_3$ NCs: (a) TEM image and (b) FE-STEM micrograph.

faces of crystalline Mo.[48,49] The magnetic constituents exhibit marked indices at (311), (400), and (440).[47] Moreover, the Raman spectra of mag-$MoO_3$ NCs shown in Figure S10B displayed typical $Mo_3$−O and $Mo_2$−O vibrations at 776 and 820 $cm^{-1}$, respectively, which can be attributed to the Mo component of the NCs.[41]

On the other hand, a uniformly SLGO-coated glass substrate was characterized by measuring the Raman absorption of the SLGO before and after conjugation of the anti-NoV antibody (NS14) and the Raman reporter (4-MBA). Figure 5a(i) shows the Raman spectra of the SLGO-coated glass substrate with the characteristic D- and G-bands of the graphene sheet appearing at 1346 and 1597 $cm^{-1}$, respectively. This observation confirms the successful coating of SLGO on the glass substrate (a detailed discussion of the uniformity of the SLGO substrate and its impact on the immunoassay is provided in S3 and Figure S2 in the Supporting Information). Furthermore, the SLGO-4MBA substrate was characterized, and the Raman spectra shown in Figure 5a(iii) revealed distinctly marked absorption peaks with significantly enhanced intensity compared to that with 4-MBA alone on a bare glass substrate (Figure 5a(ii)). Graphene nanostructures (SLGO) are known to display surface plasmons in the terahertz range.[20,50] Hence, the observed Raman intensity increase in 4-MBA-conjugated SLGO indicates the SERS enhancement properties of SLGO alone without mag-$MoO_3$ NCs. The peak of 4-MBA at 1096 $cm^{-1}$ was enhanced by $10^5$-fold (Table S1 in the Supporting Information). Similarly, the desired signal-monitoring peak of the reporter at 1596 $cm^{-1}$ displayed $10^5$-fold enhancement coupled with significant broadening of the absorption peak due to the close/combined absorption of the G-band of SLGO and 4-MBA and not necessarily due to background signals.

Moreover, the D-band of the SLGO shifted slightly because of the conjugation of the 4-MBA/antibody to the SLGO.[51,52] This conjugation may also be responsible for the new absorption peak appearing at ∼1452 $cm^{-1}$ (Figure 5a(iii)), as this peak is absent in the Raman spectrum of the 4-MBA molecule alone (Figure 5a(ii)). These results confirm the successful fabrication of the various graphene-based SLGO capture/substrate platforms and demonstrate their SERS activities by significant enhancement of the Raman signal of 4-MBA.

**3.4. Immunospecificity and Sandwich Complex Characterization.** The biological specificity and binding ability of the anti-NoV antibody to the NoV antigen/NoV-VLPs and the ability to form sandwich immunocomplexes have been previously studied using ELISA (S8 and Figure S11 in the Supporting Information).[53,54] Accordingly, the prepared antibody-mag-$MoO_3$ NCs have been proven to exhibit biological specificity and high activity toward NoV/NoV-LPs (S9 in the Supporting Information). The antibody-mag-$MoO_3$ NC conjugate demonstrated specific binding affinity for the target NoV-LPs based on the marked difference in absorption compared to that of other viruses and virus-like particles (Figure S12 in the Supporting Information). Ideally, to achieve sensitive detection, the minimum amount of antibody conjugation to mag-$MoO_3$ NCs is needed for an effective immunoreaction with NoV-LPs/NoV. As a result, the amount of anti-NoV antibodies bound to the mag-$MoO_3$ NCs


https://dx.doi.org/10.1021/acsami.0c14729
ACS Appl. Mater. Interfaces XXXX, XXX, XXX−XXX

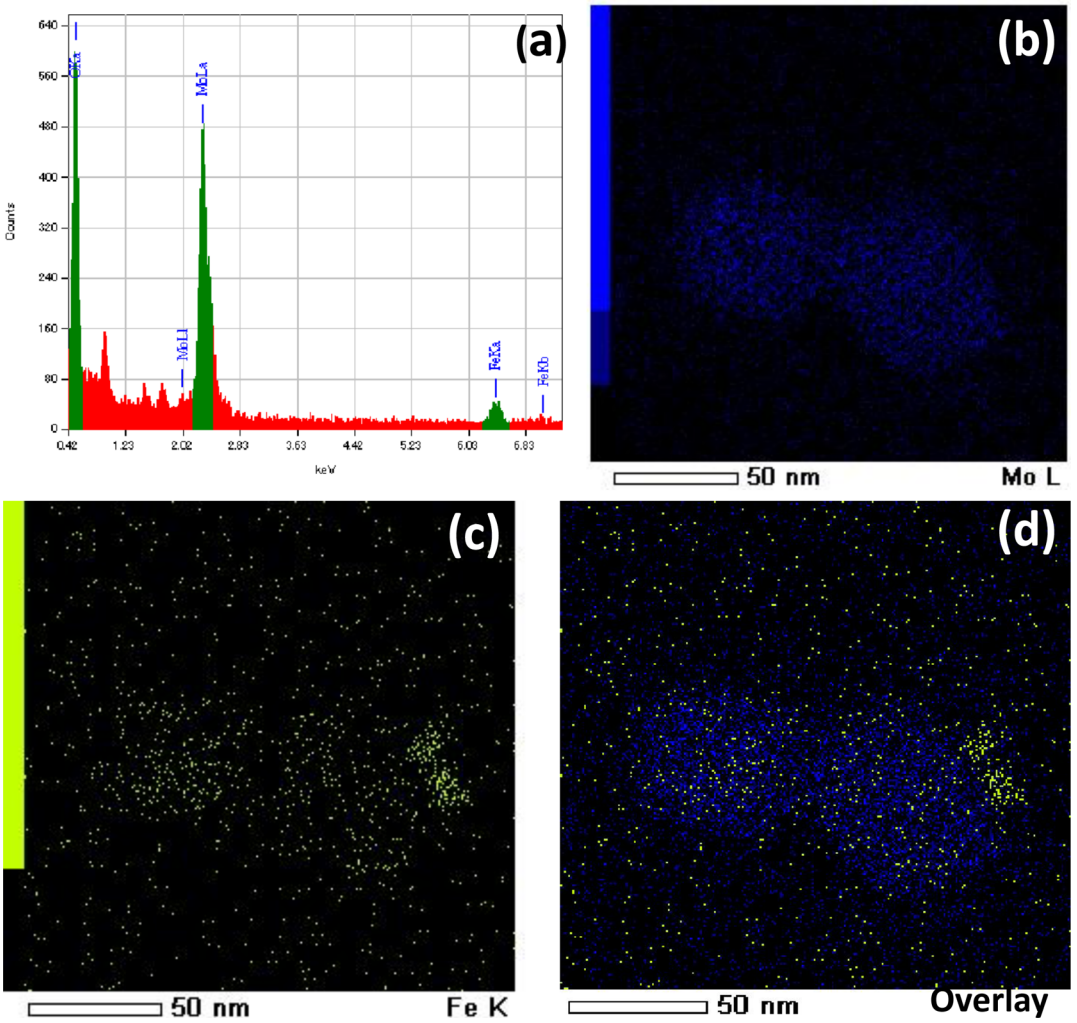


**Figure 3.** (a) Elemental X-ray dispersive spectra of mag-$MoO_3$ NCs and mapping spectra of (b) Mo, (c) Fe, and (d) merged (overlay).

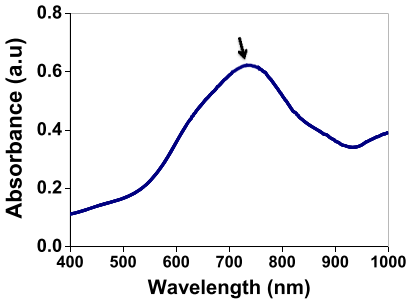


**Figure 4.** UV−vis absorption spectrum of mag-$MoO_3$ NCs showing the LSPR peak at ∼738 nm.

estimated by the indirect approach was found to be ∼5 × $10^2$ $\mu$g/mag-$MoO_3$ NCs, corresponding to ∼12% of the mag-$MoO_3$ NC surface coverage (S10, Supporting Information). The immobilization efficiency achieved can be considered adequate as a higher percentage binding of the antibodies can potentially reduce the antigen recognition efficiency of antibody-mag-$MoO_3$ NCs and make them less accessible to NoV/NoV-LPs because of the steric hindrance between nearby antibodies.[55,56] Details on the sandwich immunocomplex/binding avidity of the monoclonal antibody (NS14) are discussed in the Supporting Information, S11.

Furthermore, the changes in the hydrodynamic size of the antibody-conjugated mag-$MoO_3$ NCs were evaluated. It was found that the hydrodynamic size of the mag-$MoO_3$ NCs increased to ∼105 nm upon antibody conjugation, compared to ∼95 nm for the mag-$MoO_3$ NCs alone (Figure S9A, Supporting Information). The sandwich immunocomplex formed between the SLGO-4MBA-antibody and antibody-mag-$MoO_3$ NCs in the presence of NoV-LPs was visualized under a transmission electron microscope (Figure 5b). The TEM image is not clear enough to indicate the sandwich nanocomplex formation because it was performed in solution without adequate staining. However, the nonspecific positioning of mag-$MoO_3$ NCs on the SLGO sheet may be seen, and the NoV appears less visible, probably due to inadequate staining or their smaller size (∼30 nm) than that of the cubic nanocrystals or SLGO nanosheets.

**3.5. SERS Signal-Amplified Immunoassay.** NoV-LPs were thus separately detected in water (PBS, 7.6) and human serum media. A sandwich-based immunoassay model similar to ELISA was implemented but with SLGO and/or 4-MBA Raman signals used for monitoring. The immunoassay sandwich protocol was performed in two separate procedures. The first approach was the direct capture of the target NoV-LPs on SLGO-based capture platforms (SLGO-antibody or SLGO-4MBA-antibody), followed by the addition of the


https://dx.doi.org/10.1021/acsami.0c14729
ACS Appl. Mater. Interfaces XXXX, XXX, XXX−XXX

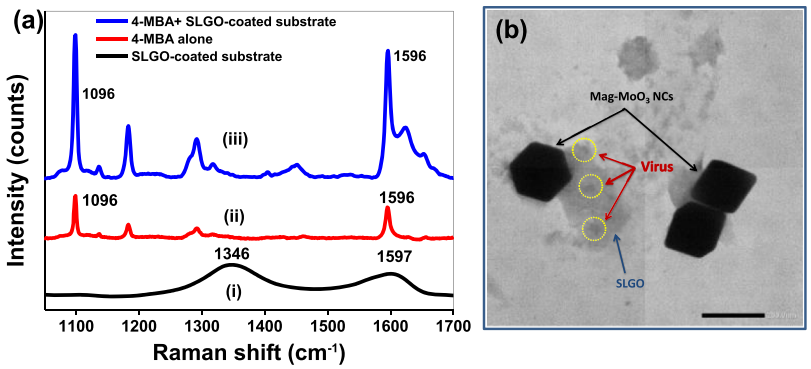


**Figure 5.** (a) Raman spectra of the (i) SLGO capture substrate, (ii) 4-MBA on a bare glass slide, and (iii) SLGO-4MBA substrate. (b) TEM image of the sandwich-type immunocomplex of mag-$MoO_3$/NoV-LPs/4-MBA-antibody-SLGO.

antibody-mag-$MoO_3$ NCs for sandwich immunocomplex formation. The second approach was a more favorable approach for the immunoassay of the target NoV/NoV-LPs in samples with complex matrices (human serum and feces). This process involved the initial capture and enrichment of the target NoV/NoV-LPs by an immunomagnetic separation protocol using the magnetic functionality of the mag-$MoO_3$ NCs, as shown in Scheme 2. Then, the magnetically enriched

**Scheme 2. Graphical Illustration of the NoV Detection Protocol in Human Feces Showing the Immunomagnetic Capture and Separation of NoV by Antibody-mag-$MoO_3$ NCs and Incubation of the NoV-Captured Antibody-mag-$MoO_3$ NCs for a Sandwich Construct on the SLGO-4MBA-Antibody Capture Substrate for SERS Immunoassay**

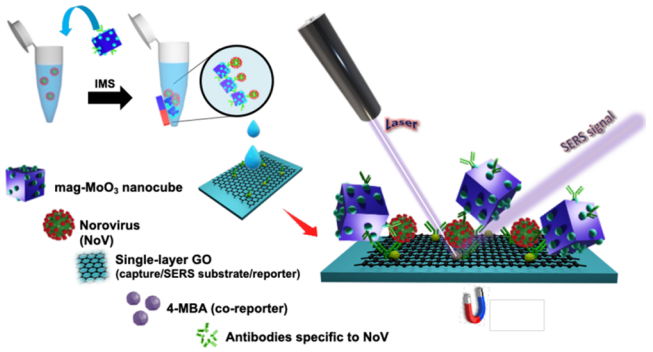


NoV-LP-antibody-mag-$MoO_3$ NC immunocomplexes were incubated on the SLGO-based platform for immunoreaction to form sandwich immunocomplexes. The first approach is quite simple and straightforward but is not ideal for clinical sample immunoassays, such as the human feces assay in this study. Hence, for NoV detection in fecal samples collected from infected patients, the second detection protocol was largely adopted.

First, the detection protocol (sandwich immunoassay) was validated using NoV-LPs prepared in DI water (PBS, pH 7.6) as the detection medium. The dynamic linear detection range and the sensitivity of the immunoassay were investigated using various concentrations of the target NoV-LPs. To do so, aliquots of the NoV-LPs were incubated on the SLGO-antibody (or SLGO-4MBA-antibody) capture substrates within the concentration range of 10 fg/mL to 1 ng/mL with an optimized detection protocol. Then, antibody-mag-$MoO_3$ NCs were incubated with the NoV-LP-captured SLGO-antibody (or SLGO-4MBA-antibody) substrates to form sandwich immunocomplexes. The formed immunocomplexes were rinsed twice with PBS (pH 7.6) under an external magnetic field before SERS measurements. Subsequently, the Raman spectra of the SLGO or SLGO-4MBA substrates were collected in the presence of different concentrations of the NoV-LPs. The results obtained show that by increasing the concentration of NoV-LPs (10 fg/mL to 100 ng/mL), the Raman intensities gradually increased for the SLGO (Figure 6a) and SLGO-4MBA substrates (4-MBA is an additional reporter) (Figure 6b). The background signals (black line spectra in Figure 6a,b) represent the signals of the reporters (SLGO or SLGO-MBA) alone without the plasmonic $MoO_3$ NCs or NoV-LPs. Then, the SERS enhancement/resonance due to the presence of NoV-LPs showed that more sandwich immunocomplexes were likely formed due to the increased capture of additional SERS-active antibody-mag-$MoO_3$ NCs arising from the sequential increase in the NoV-LPs concentration.

Interestingly, the SLGO-based capture substrate presents a large surface area on which the antibody-mag-$MoO_3$ NCs can be accommodated very close to the surface of the SLGO-antibody (SLGO-4MBA-antibody) platform to enhance the Raman signal of the SLGO or 4-MBA via an electromagnetic mechanism. In addition, SLGO can further boost the signals of covalently bound 4-MBA via a chemical mechanism.[20,21,27] As a quantitative measure of the levels of the target NoV-LPs, the calibration plot for NoV-LPs detection was constructed using the enhanced SERS signals of SLGO. The calibration plots constructed using the characteristic D- and G-bands of SLGO at 1348 and 1597 $cm^{-1}$, respectively, are shown in Figure 6c. Calibration plots were also generated for the SLGO-4MBA capture platform as a function of the SERS intensity versus NoV-LP concentration (Figure 6d). The Raman intensities for ten replicate measurements were averaged for each concentration, and the error bars display the default variances of the replicate measurements ($n$ = 10). Using log−log transformation,[57,58] linear plots were obtained, which show strong linear dynamic responses in the range of 10 pg/mL to 100 ng/mL for the SLGO-antibody capture/substrate platform. Exhibiting a higher sensitivity, the SLGO-4MBA-antibody platform showed linear responses within 10 fg/mL to 1 ng/mL. The LODs for the NoV-LPs were calculated to be ~2.5 pg/mL and 5.2 fg/mL in PBS (pH 7.6) for the SLGO and SLGO-4MBA reporter systems, respectively. The LOD was calculated using (LOD = $3\delta/K$),[42] where $\delta$ represents the standard deviation ($n$ = 10) and $K$ represents the value of the slopes of the linear calibration plot. Further discussion and


https://dx.doi.org/10.1021/acsami.0c14729
ACS Appl. Mater. Interfaces XXXX, XXX, XXX−XXX

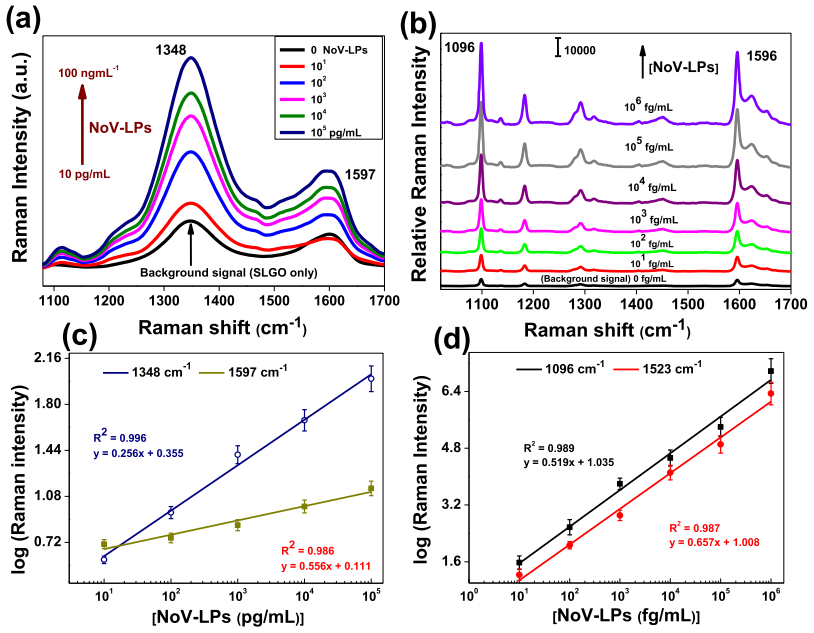


**Figure 6.** SERS-based detection of NoV-LPs using the (a) SLGO-antibody substrate (SLGO as a reporter) and (b) SLGO-4-MBA-antibody substrate (4-MBA as a reporter). Corresponding calibration plots of (c) Raman D- and G-bands of SLGO at 1348 and 1597 $cm^{-1}$, respectively, and (d) Raman D- and G-bands of 4-MBA at 1098 and 1596 $cm^{-1}$, respectively. The SLGO or 4-MBA signals (black line spectra) in (a,b) are the background signals (at 0 fg/mL of NoV-LPs).

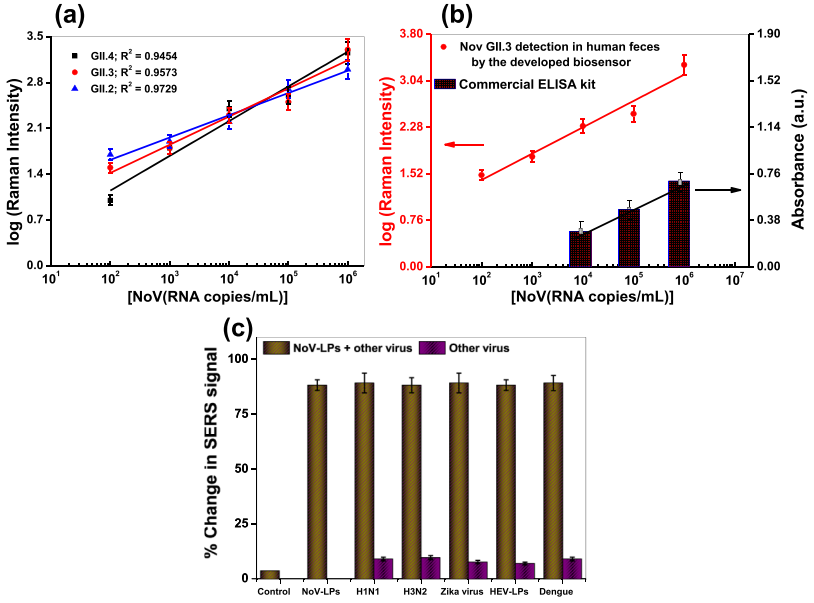


**Figure 7.** SERS-based dual nanotag/substrate biosensing system for NoV. (a) Calibration plots for the detection of NoV subtypes in human feces. (b) Comparison of the detection performance of the developed biosensor (red line) with that of a commercial ELISA kit, NV-EIA (black line). (c) Specific detection of NoV in the presence of other viruses and virus-like particles.

calibration plots for NoV-LPs detection in human serum are provided in S12 and Figure S13 in the Supporting Information.

Comparing the results obtained using the SLGO and SLGO-4MBA reporter systems; the SLGO-4MBA system presents a higher sensitivity for NoV-LPs quantitation. According to a previous report, the number of particles of NoV-LPs was measured to be approximately $4.3 \times 10^5$ particles/mL in ~10 pg/mL NoV-LPs. Therefore, the obtained LODs of 2.5 pg/mL (SLGO-antibody system) and 5.2 fg/mL (SLGO-4MBA-antibody system) in this work correspond to the detectability of ~$10^2$ and $10^5$ particles/mL NoV-LPs, respectively. The plausible reason for the different detection sensitivities may be due to the synergistic SERS enhancement mechanisms from the plasmonic mag-$MoO_3$ NCs coupled with the chemical enhancement mechanism contributed by SLGO to the 4-MBA molecule. The results also show that the bare SLGO platform provides competitive flexibility and sensitivity compared with the use of an external classical Raman reporter. Hence, the SLGO capture platform can be solely adopted without the need for 4-MBA.

**3.6. Clinical NoV Detection in Human Feces.** To eliminate or reduce interferences usually encountered in real


https://dx.doi.org/10.1021/acsami.0c14729
ACS Appl. Mater. Interfaces XXXX, XXX, XXX−XXX

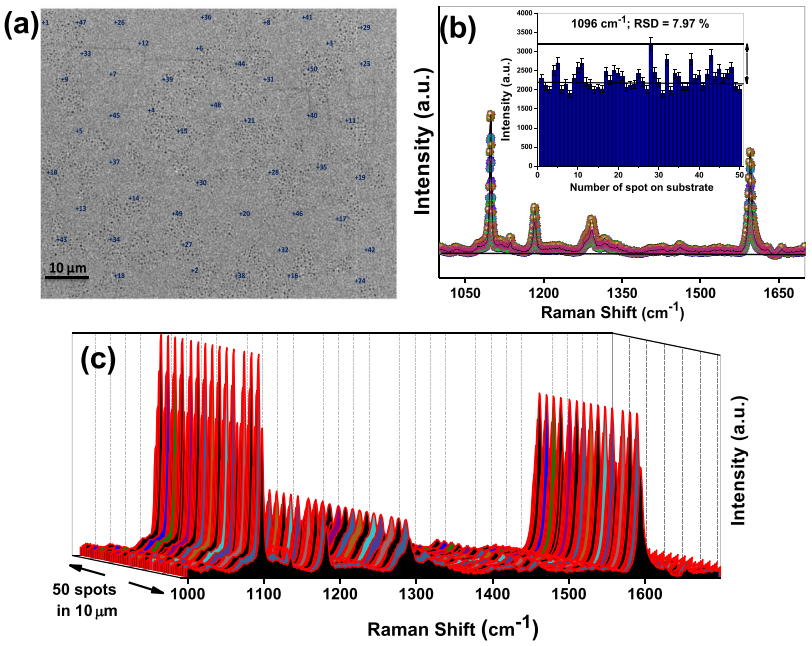


**Figure 8.** SERS mapping image results: (a) randomly selected 50 spots on the substrate and (b) overlapped SERS spectra of 4-MBA induced by 1 ng/mL NoV collected at over 50 random spots on the substrate. The inset shows the spot-to-spot SERS intensity variation for the 4-MBA peak at 1096 $cm^{-1}$. (c) Displayed collective SERS spectra of 4-MBA for all randomly distributed spots.

sample immunoassays, an immunomagnetic separation protocol for the capture/enrichment of NoV in human feces was adopted.[20,30] Here, the magnetic functionality of the mag-$MoO_3$ NCs proved useful by the initial immunocomplex of different concentrations of NoV with antibody-mag-$MoO_3$ NCs and their subsequent magnetic separation before deposition on the capture substrate. Several clinical NoV subtypes (GII.2, GII.3, and GII.4) from the human feces of infected patients were tested using this system to prove the practical application of the developed SERS-based immunoassay. For all the RNA subtypes assayed, positive SERS responses were obtained within $10^2$ to $10^6$ RNA copies/mL (using the SLGO-4MBA antibody), as shown in Figure 7a. The results obtained for NoV detection show that GII.2 and GII.3, with LODs of 60 RNA copies/mL and 96 RNA copies/mL, respectively, were the most sensitively detected. By comparison, G11.4 was the least sensitively detected, with an LOD of 180 RNA copies/mL.

Furthermore, comparing the performance of the developed biosensor with that of a commercial ELISA kit for NoV detection, the proposed biosensor detected the NoV subtypes in fecal samples with an LOD of ~60 RNA copies/mL within a linear dynamic range of $10^2$ to $10^6$ copies/mL, compared to $10^4$ to $10^6$ copies/mL NoV viral RNA detectable by the ELISA kit (Figure 7b) (LOD = $1.65 \times 10^4$) and $\geq 10^6$ copies/mL detectable by the lateral flow kit (LOD = $3.5 \times 10^6$). This result shows that our developed biosensor has significantly higher sensitivity (on the order of ~$10^3$ and $\geq 10^5$) than the commercial ELISA kit and the lateral flow kit, respectively. In comparison to previous detection systems (Table S2 in the Supporting Information), this system holds promising prospects for significant improvements in the detection of NoV in clinical samples.

**3.7. Specificity and Selectivity.** The selectivity of the developed biosensor for NoV was probed separately in the presence of influenza viruses A/H1N1 and A/H3N2, Zika virus, hepatitis E virus (HEV-LPs), and dengue DNA. As shown in Figure 7c, insignificant changes in SERS signals occurred at 10 ng/mL of the tested viruses and virus-like particles. This observation can be attributed to the specific affinity of NoV to jointly bind to the antibody-functionalized SERS substrates. It is also pertinent to state here that this detection system, which is based on antibody-mag-$MoO_3$ NCs and SLGO-antibody (or SLGO-4MBA-antibody) capture substrates, might present a flexible target virus detection approach. It is possible to detect target viruses by selecting a suitable antigen−antibody pair for sandwich-type immunoreactions. The study of the stable immunocomplex formation of the biosensor is presented in S13 and Figure S14 (Supporting Information). In addition, the effects of the magnetic field on the SERS of the biosensor are discussed in S14 and Figure S15 (Supporting Information).

**3.8. Reproducibility of the Dual SERS Nanotag/Substrate.** The reproducibility of the developed NoV biosensor was studied as a parameter necessary for performance evaluation and robustness. The ability of the SLGO substrates to produce reproducible Raman signals was demonstrated, as discussed in S3 and Figure S2 in the Supporting Information. Hence, the reproducibility of the SERS signals of the biosensor was tested using 1 ng/mL NoV-LPs to collate the mean intensity of generated SERS signals from 50 spots randomly mapped onto the substrate (Figure 8a,c). These values were obtained using the 4-MBA Raman peak at 1096 $cm^{-1}$. The results showed that in all the spots tested, each spot can generate a good SERS signal, albeit with some differences in signal intensities, which is quite expected. To further estimate the uniformity and reproducibility of the SERS signals, the relative standard deviation (RSD) of the signals from the mean intensity was calculated. The calculated RSD for the SERS signals using the peak at 1096 $cm^{-1}$ (4-MBA) was ~7.95% (Figure 8b). The RSD at 1598 $cm^{-1}$ was ~8.67%. The RSDs at these measurements being less than or


https://dx.doi.org/10.1021/acsami.0c14729
ACS Appl. Mater. Interfaces XXXX, XXX, XXX−XXX

slightly more than 8% are an indication of the excellent spot-to-spot reproducibility[59] of the SLGO-4MBA substrate.

Furthermore, the number of "hotspots" was estimated using the statistical ratio of the mapped large area (50 $\mu$m × 50 $\mu$m) on the substrate at 1096 $cm^{-1}$ (Figure S15A in the Supporting Information). The data obtained from the multipoint scans were used to estimate the coverage of the active SERS regions on the capture platform using the least-squares (LS) algorithm.[60,61] In Figure 9, the relative number of "hotspots"

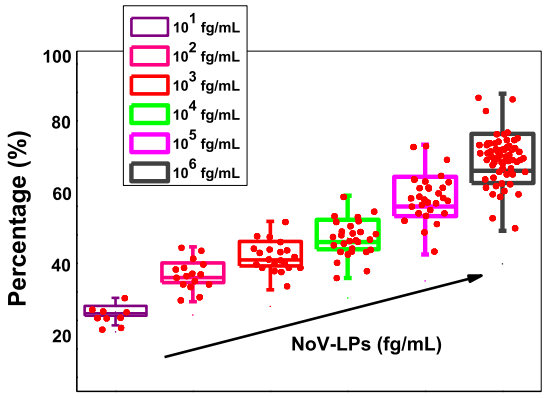


**Figure 9.** Statistical estimation of the number of "hotspots" as a function of the amount of NoV-induced sandwiched constructs. Each box represents the approximate area of the mapped region and is placed according to the percentage of SERS intensities measured and their estimated distribution (upper, median, and lower limits).

on the SERS capture platform is shown, and the effective distribution of the "hotspots" is skewed to higher intensity values depending on the target NoV-LP concentration (10 fg/mL to 1 ng/mL).

## 4. CONCLUSIONS

As a major research stimulus, G-SERS-based diagnostic technologies have facilitated high-level ultrasensitive single-molecule detection via "hotspot" engineering. In this study, a novel dual SERS nanotag/substrate immunoassay was developed based on the cooperative effects of the optical properties of new magnetic-functionalized $MoO_3$ NCs on an SLGO capture/substrate platform for NoV detection. Owing to the magnetic separation protocol adopted, NoV was enriched and separated from human fecal clinical samples and detected within a linear dynamic detection range of $10^2$ to $10^6$ RNA copies/mL. The critical determinant of the developed biosensor's performance is the accuracy of the antigen−antibody interactions to form a sandwich immunocomplex. Nonetheless, the carefully engineered uniformity of the SLGO substrate and application of a magnetic force are also determining factors in the sensitivity of the assay. Overall, this study demonstrates that advances in nanofabrication and "hotspot" engineering technology can help implement new diagnostic technologies needed to improve sensitive SERS-based immunoassays of infectious diseases. For this particular study, by integrating a portable/handheld Raman spectrometer, the prospects of engineering a POC biosensor for NoV using this system may be accomplished.

## ASSOCIATED CONTENT

### Supporting Information

The Supporting Information is available free of charge at https://pubs.acs.org/doi/10.1021/acsami.0c14729.

Scheme of SLGO capture substrate preparation and uniformity characterization, SERS properties of the dual SERS nanotag/substrate, control study discussion and data, Raman enhancement factors (EFs) of substrates and the comparison of some NoV detection systems with the developed biosensor, TEM image of mag-$MoO_3$ NC synthesis stage, DLS, zeta potential data (antibody-mag-$MoO_3$ NCs), XRD and Raman spectra of mag-$MoO_3$ NCs, ELISA tests for antibody-binding studies and the number of NoV antibodies bound to mag-$MoO_3$ NCs, LOD comparison, aggregation index (AI) of the formed sandwich nanostructures and the corresponding calibration plots for NoV-LPs detection in 5% human serum (probability distribution function), and the effects of magnetic force field on the SERS immunoassay (PDF)

## AUTHOR INFORMATION

### Corresponding Author

**Enoch Y. Park** − *Research Institute of Green Science and Technology and Laboratory of Biotechnology, Department of Bioscience, Graduate School of Science and Technology, Shizuoka University, Shizuoka 422-8529, Japan;* orcid.org/0000-0002-7840-1424; Phone: +81-54-238-4887; Email: park.enoch@shizuoka.ac.jp

### Authors

**Ojodomo J. Achadu** − *Research Institute of Green Science and Technology, Shizuoka University, Shizuoka 422-8529, Japan*

**Fuyuki Abe** − *Department of Microbiology, Shizuoka Institute of Environment and Hygiene, Fujieda 426-0083, Japan*

**Tetsuro Suzuki** − *Department of Infectious Diseases, Hamamatsu University School of Medicine, Hamamatsu 431-3192, Japan*

Complete contact information is available at: https://pubs.acs.org/10.1021/acsami.0c14729

### Notes

The authors declare no competing financial interest.

## ACKNOWLEDGMENTS

O.J.A. gratefully thanks the Japan Society for the Promotion of Science (JSPS) for a Postdoctoral Fellowship for Research in Japan (Standard) (grant no. 19F19348).

## REFERENCES

(1) Ao, Y.; Xie, X.; Dong, X.; Jin, M.; Duan, Z. Genetic Analysis of an Emerging GII.P2−GII.2 Norovirus Associated with a 2016 Outbreak of Acute Gastroenteritis in China. *Virol. Sin.* **2019**, *34*, 111−114.

(2) Patel, M. M.; Hall, A. J.; Vinjé, J.; Parashar, U. D. Noroviruses: A Comprehensive Review. *J. Clin. Virol.* **2009**, *44*, 1−8.

(3) Vinjé, J. Advances in Laboratory Methods for Detection and Typing of Norovirus. *J. Clin. Microbiol.* **2015**, *53*, 373−381.

(4) Liu, L.; Moore, M. D. A Survey of Analytical Techniques for Noroviruses. *Foods* **2020**, *9*, 318.

(5) Granger, J. H.; Schlotter, N. E.; Crawford, A. C.; Porter, M. D. Prospects for Point-of-Care Pathogen Diagnostics Using Surface-



https://dx.doi.org/10.1021/acsami.0c14729
ACS Appl. Mater. Interfaces XXXX, XXX, XXX−XXX

Enhanced Raman Scattering (SERS). *Chem. Soc. Rev.* **2016**, *45*, 3865−3882.
(6) Wang, C.; Wang, C.; Wang, X.; Wang, K.; Zhu, Y.; Rong, Z.; Wang, W.; Xiao, R.; Wang, S. Magnetic SERS Strip for Sensitive and Simultaneous Detection of Respiratory Viruses. *ACS Appl. Mater. Interfaces* **2019**, *11*, 19495−19505.
(7) Nagy-Simon, T.; Tatar, A. S.; Craciun, A. M.; Vulpoi, A.; Jurj, M. A.; Florea, A.; Tomuleasa, C.; Berindan-Neagoe, I.; Astilean, S.; Boca, S. Antibody Conjugated, Raman Tagged Hollow Gold-Silver Nanospheres for Specific Targeting and Multimodal Dark-Field/SERS/Two Photon-FLIM Imaging of CD19(+) B Lymphoblasts. *ACS Appl. Mater. Interfaces* **2017**, *9*, 21155−21168.
(8) Kaminska, A.; Witkowska, E.; Winkler, K.; Dziecielewski, I.; Weyher, J. L.; Waluk, J. Detection of Hepatitis B Virus Antigen from Human Blood: SERS Immunoassay in a Microfluidic System. *Biosens. Bioelectron.* **2015**, *66*, 461−467.
(9) Shao, F.; Lu, Z.; Liu, C.; Han, H.; Chen, K.; Li, W.; He, Q.; Peng, H.; Chen, J. Hierarchical Nanogaps within Bioscaffold Arrays as a High-Performance SERS Substrate for Animal Virus Biosensing. *ACS Appl. Mater. Interfaces* **2014**, *6*, 6281−6289.
(10) Cao, Y. C.; Jin, R.; Nam, J.-M.; Thaxton, C. S.; Mirkin, C. A. Raman Dye-Labeled Nanoparticle Probes for Proteins. *J. Am. Chem. Soc.* **2003**, *125*, 14676.
(11) Zhang, S.-B.; Wu, Z.-S.; Guo, M.-M.; Shen, G.-L.; Yu, R.-Q. A Novel Immunoassay Strategy Based on Combination of Chitosan and a Gold Nanoparticle Label. *Talanta* **2007**, *71*. DOI: DOI: 10.1016/j.talanta.2006.07.036.
(12) Wang, Y.; Schlücker, S. Rational Design and Synthesis of SERS Labels. *Analyst* **2013**, *138*, 2224.
(13) Li, M.; Cushing, S. K.; Zhang, J.; Lankford, J.; Aguilar, Z. P.; Ma, D.; Wu, N. Shape-Dependent Surface-Enhanced Raman Scattering in Gold-Raman-Probe- Silica Sandwiched Nanoparticles for Biocompatible Applications. *Nanotechnology* **2012**, *23*, 115501.
(14) Gong, J.-L.; Liang, Y.; Huang, Y.; Chen, J.-W.; Jiang, J.-H.; Shen, G.-L.; Yu, R.-Q. Ag/SiO2 Core-Shell Nanoparticle-Based Surface-Enhanced Raman Probes for Immunoassay of Cancer Marker Using Silica-Coated Magnetic Nanoparticles as Separation Tools. *Biosens. Bioelectron.* **2007**, *22*. DOI: DOI: 10.1016/j.bios.2006.07.004.
(15) Ouyang, L.; Ren, W.; Zhu, L.; Irudayaraj, J. Prosperity to Challenges: Recent Approaches in SERS Substrate Fabrication. *Rev. Anal. Chem.* **2017**, *36*, 20160027.
(16) Tang, H.; Zhu, C.; Meng, G.; Wu, N. Review—Surface-Enhanced Raman Scattering Sensors for Food Safety and Environmental Monitoring. *J. Electrochem. Soc.* **2018**, *165*, B3098−B3118.
(17) Grubisha, D. S.; Lipert, R. J.; Park, H.-Y.; Driskell, J.; Porter, M. D. Femtomolar Detection of Prostate-Specific Antigen: An Immunoassay Based on Surface-Enhanced Raman Scattering and Immunogold Labels. *Anal. Chem.* **2003**, *75*, 5936.
(18) Porter, M. D.; Lipert, R. J.; Siperko, L. M.; Wang, G.; Narayanan, R. SERS as a Bioassay Platform: Fundamentals, Design, and Applications. *Chem. Soc. Rev.* **2008**, *37*, 1001.
(19) Lee, H. K.; Lee, Y. H.; Koh, C. S. L.; Phan-Quang, G. C.; Han, X.; Lay, C. L.; Sim, H. Y. F.; Kao, Y.-C.; An, Q.; Ling, X. Y. Designing Surface-Enhanced Raman Scattering (SERS) Platforms beyond Hotspot Engineering: Emerging Opportunities in Analyte Manipulations and Hybrid Materials. *Chem. Soc. Rev.* **2019**, *48*, 731.
(20) Kang, L.; Chu, J.; Zhao, H.; Xu, P.; Sun, M. Recent Progress in the Applications of Graphene in Surface-Enhanced Raman Scattering and Plasmon-Induced Catalytic Reactions. *J. Mater. Chem. C* **2015**, *3*, 9024−9037.
(21) Ling, X.; Xie, L.; Fang, Y.; Xu, H.; Zhang, H.; Kong, J.; Dresselhaus, M. S.; Zhang, J.; Liu, Z. Can Graphene Be Used as a Substrate for Raman Enhancement? *Nano Lett.* **2010**, *10*, 553.
(22) Wang, P.; Zhang, D.; Zhang, L.; Fang, Y. The SERS Study of Graphene Deposited by Gold Nanoparticles with 785 nm Excitation. *Chem. Phys. Lett.* **2013**, *556*, 146.
(23) Song, D.; Yang, R.; Long, F.; Zhu, A. Applications of Magnetic Nanoparticles in Surface-Enhanced Raman Scattering (SERS) Detection of Environmental Pollutants. *J. Environ. Sci.* **2019**, *80*, 14.
(24) Kou, B.; Huang, W.; Neill, F. H.; Palzkill, T.; Estes, M. K.; Atmar, R. L. Norovirus Antigen Detection with a Combination of Monoclonal and Single-Chain Antibodies. *J. Clin. Microbiol.* **2015**, *53*, 3916−3918.
(25) Ahmed, S. R.; Takemeura, K.; Li, T.-C.; Kitamoto, N.; Tanaka, T.; Suzuki, T.; Park, E. Y. Size-Controlled Preparation of Peroxidase-like Graphene-Gold Nanoparticle Hybrids for the Visible Detection of Norovirus-like Particles. *Biosens. Bioelectron.* **2017**, *87*, 558−565.
(26) Li, T. C.; Yamakawa, Y.; Suzuki, K.; Tatsumi, M.; Razak, M. A.; Uchida, T.; Takeda, N.; Miyamura, T. Expression and Self-Assembly of Empty Virus-like Particles of Hepatitis E Virus. *J. Virol.* **1997**, *71*, 7207−7213.
(27) Zhou, X.; Huang, X.; Qi, X.; Wu, S.; Xue, C.; Boey, F. Y. C.; Yan, Q.; Chen, P.; Zhang, H. In Situ Synthesis of Metal Nanoparticles on Single-Layer Graphene Oxide and Reduced Graphene Oxide Surfaces. *J. Phys. Chem. C* **2009**, *113*, 10842−10846.
(28) Langer, J.; Jimenez de Aberasturi, D.; Aizpurua, J.; Alvarez-Puebla, R. A.; Auguié, B.; Baumberg, J. J.; Bazan, G. C.; Bell, S. E. J.; Boisen, A.; Brolo, A. G.; Choo, J.; Cialla-May, D.; Deckert, V.; Fabris, L.; Faulds, K.; García de Abajo, F. J.; Goodacre, R.; Graham, D.; Haes, A. J.; Haynes, C. L.; Huck, C.; Itoh, T.; Käll, M.; Kneipp, J.; Kotov, N. A.; Kuang, H.; Le Ru, E. C.; Lee, H. K.; Li, J.-F.; Ling, X. Y.; Maier, S. A.; Mayerhöfer, T.; Moskovits, M.; Murakoshi, K.; Nam, J.-M.; Nie, S.; Ozaki, Y.; Pastoriza-Santos, I.; Perez-Juste, J.; Popp, J.; Pucci, A.; Reich, S.; Ren, B.; Schatz, G. C.; Shegai, T.; Schlücker, S.; Tay, L.-L.; Thomas, K. G.; Tian, Z.-Q.; Van Duyne, R. P.; Vo-Dinh, T.; Wang, Y.; Willets, K. A.; Xu, C.; Xu, H.; Xu, Y.; Yamamoto, Y. S.; Zhao, B.; Liz-Marzán, L. M. Present and Future of Surface-Enhanced Raman Scattering. *ACS Nano* **2019**, *14*, 28−117.
(29) Kumari, G.; Kandula, J.; Narayana, C. How Far Can We Probe by SERS? *J. Phys. Chem. C* **2015**, *119*, 20057.
(30) Neng, J.; Harpster, M. H.; Wilson, W. C.; Johnson, P. A. Surface-Enhanced Raman Scattering (SERS) Detection of Multiple Viral Antigens Using Magnetic Capture of SERS-Active Nanoparticles. *Biosens. Bioelectron.* **2013**, *41*, 316−321.
(31) Sun, Y.; Xu, L.; Zhang, F.; Song, Z.; Hu, Y.; Ji, Y.; Shen, J.; Li, B.; Lu, H.; Yang, H. A Promising Magnetic SERS Immunosensor for Sensitive Detection of Avian Influenza Virus. *Biosens. Bioelectron.* **2017**, *89*, 906−912.
(32) Zou, F.; Zhou, H.; Tan, T. V.; Kim, J.; Koh, K.; Lee, J. Dual-Mode SERS-Fluorescence Immunoassay Using Graphene Quantum Dot Labeling on One-Dimensional Aligned Magnetoplasmonic Nanoparticles. *ACS Appl. Mater. Interfaces* **2015**, *7*, 12168−12175.
(33) Ranc, V.; Markova, Z.; Hajduch, M.; Prucek, R.; Kvitek, L.; Kaslik, J.; Safarova, K.; Zboril, R. Magnetically Assisted Surface-Enhanced Raman Scattering Selective Determination of Dopamine in an Artificial Cerebrospinal Fluid and a Mouse Striatum Using Fe3O4/Ag Nanocomposite. *Anal. Chem.* **2014**, *86*, 2939.
(34) Chen, M.; Luo, W.; Zhang, Z.; Wang, R.; Zhu, Y.; Yang, H.; Chen, X. Synthesis of Multi-Au-Nanoparticle-Embedded Mesoporous Silica Microspheres as Self-Filtering and Reusable Substrates for SERS Detection. *ACS Appl. Mater. Interfaces* **2017**, *9*, 42156.
(35) Pham, X.-H.; Hahm, E.; Huynh, K.-H.; Son, B. S.; Kim, H.-M.; Jeong, D. H.; Jun, B.-H. 4-Mercaptobenzoic Acid Labeled Gold-Silver-Alloy-Embedded Silica Nanoparticles as an Internal Standard Containing Nanostructures for Sensitive Quantitative Thiram Detection. *Int. J. Mol. Sci.* **2019**, *20*, 4841.
(36) Chen, M.-C.; Yang, Y.-L.; Chen, S.-W.; Li, J.-H.; Aklilu, M.; Tai, Y. Self-Assembled Monolayer Immobilized Gold Nanoparticles for Plasmonic Effects in Small Molecule Organic Photovoltaic. *ACS Appl. Mater. Interfaces* **2013**, *5*, 511.
(37) Pham, X.-H.; Hahm, E.; Kang, E.; Son, B.; Ha, Y.; Kim, H.-M.; Jeong, D.; Jun, B.-H. Control of Silver Coating on Raman Label Incorporated Gold Nanoparticles Assembled Silica Nanoparticles. *Int. J. Mol. Sci.* **2019**, *20*, 1258.


https://dx.doi.org/10.1021/acsami.0c14729
ACS Appl. Mater. Interfaces XXXX, XXX, XXX−XXX

(38) Yu, X.; Cai, H.; Zhang, W.; Li, X.; Pan, N.; Luo, Y.; Wang, X.; Hou, J. G. Tuning Chemical Enhancement of SERS by Controlling the Chemical Reduction of Graphene Oxide Nanosheets. *ACS Nano* **2011**, *5*, 952.
(39) Ling, X.; Huang, S.; Deng, S.; Mao, N.; Kong, J.; Dresselhaus, M. S.; Zhang, J. Lighting Up the Raman Signal of Molecules in the Vicinity of Graphene Related Materials. *Acc. Chem. Res.* **2015**, *48*, 1862.
(40) Xie, S.; Zhang, H.; Liu, G.; Wu, X.; Lin, J.; Zhang, Q.; Wang, Y. Tunable Localized Surface Plasmon Resonances in MoO3−x-TiO2 Nanocomposites with Enhanced Catalytic Activity for CO2 Photoreduction under Visible Light. *Chin. J. Catal.* **2020**, *41*, 1125.
(41) Zhang, J.; Pan, Y.; Chen, Y.; Lu, H. Plasmonic Molybdenum Trioxide Quantum Dots with Noble Metal-Comparable Surface Enhanced Raman Scattering. *J. Mater. Chem. C* **2018**, *6*, 2216−2220.
(42) Jiang, X.; Yin, D.; Yang, M.; Du, J.; Wang, W.; Zhang, L.; Yang, L.; Han, X.; Zhao, B. Revealing Interfacial Charge Transfer in TiO2/Reduced Graphene Oxide Nanocomposite by Surface-Enhanced Raman Scattering (SERS): Simultaneous a Superior SERS-Active Substrate. *Appl. Surf. Sci.* **2019**, *487*, 938−944.
(43) Jiang, X.; Sang, Q.; Yang, M.; Du, J.; Wang, W.; Yang, L.; Han, X.; Zhao, B. Metal-Free SERS Substrate Based on RGO-TiO2-Fe3O4 Nanohybrid: Contribution from Interfacial Charge Transfer and Magnetic Controllability. *Phys. Chem. Chem. Phys.* **2019**, *21*, 12850.
(44) Jiang, X.; Li, X.; Jia, X.; Li, G.; Wang, X.; Wang, G.; Li, Z.; Yang, L.; Zhao, B. Surface-Enhanced Raman Scattering from Synergistic Contribution of Metal and Semiconductor in $TiO_2$/MBA/Ag(Au) and Ag(Au)/MBA/$TiO_2$ Assemblies. *J. Phys. Chem. C* **2012**, *116*, 14650.
(45) Kong, X.-k.; Chen, Q.-w.; Sun, Z.-y. Enhanced SERS of the Complex Substrate Using Au Supported on Graphene with Pyridine and R6G as the Probe Molecules. *Chem. Phys. Lett.* **2013**, *564*, 54.
(46) Zu, H.; Guo, Y.; Yang, H.; Huang, D.; Liu, Z.; Liu, Y.; Hu, C. Rapid Room-Temperature Preparation of MoO3−x Quantum Dots by Ultraviolet Irradiation for Photothermal Treatment and Glucose Detection. *New J. Chem.* **2018**, *42*, 18533−18540.
(47) Achadu, O. J.; Takemura, K.; Khoris, I. M.; Park, E. Y. Plasmonic/Magnetic Molybdenum Trioxide and Graphitic Carbon Nitride Quantum Dots-Based Fluoroimmunosensing System for Influenza Virus. *Sens. Actuators, B* **2020**, *321*, 128494.
(48) Borghei, S. M. Investigation of the Properties of Molybdenum Nanocube Crystals Deposited by Dc Sputtering. *Acta Phys. Pol., A* **2016**, *129*, 607−609.
(49) Yuan, Z.; Si, L.; Wei, D.; Hu, L.; Zhu, Y.; Li, X.; Qian, Y. Vacuum Topotactic Conversion Route to Mesoporous Orthorhombic MoO 3 Nanowire Bundles with Enhanced Electrochemical Performance. *J. Phys. Chem. C* **2014**, *118*, 5091−5101.
(50) Kanchanapally, R.; Fan, Z.; Wesley, W.; Nellore, B. P. V.; Crouch, R. A.; Sinha, S. S.; Pramanik, A.; Chavva, S. R.; Ray, P. C. Detection of Melamine from Food in Parts per Quadrillion Level Using Functionalized Graphene Oxide-Gold Nanoparticle Hybrid SERS Platform. *Food Poisoning: Outbreaks, Bacterial Sources and Adverse Health Effects*; Nova Science Publishers, 2014.
(51) Achadu, O. J.; Uddin, I.; Nyokong, T. Fluorescence Behavior of Nanoconjugates of Graphene Quantum Dots and Zinc Phthalocyanines. *J. Photochem. Photobiol., A* **2016**, *317*, 12−25.
(52) Nwahara, N.; Achadu, O. J.; Nyokong, T. In-Situ Synthesis of Gold Nanoparticles on Graphene Quantum Dots-Phthalocyanine Nanoplatforms: First Description of the Photophysical and Surface Enhanced Raman Scattering Behaviour. *J. Photochem. Photobiol., A* **2018**, *359*, 131−144.
(53) Takemura, K.; Adegoke, O.; Takahashi, N.; Kato, T.; Li, T.-C.; Kitamoto, N.; Tanaka, T.; Suzuki, T.; Park, E. Y. Versatility of a Localized Surface Plasmon Resonance-Based Gold Nanoparticle-Alloyed Quantum Dot Nanobiosensor for Immunofluorescence Detection of Viruses. *Biosens. Bioelectron.* **2017**, *89*, 998−1005.
(54) Nasrin, F.; Chowdhury, A. D.; Takemura, K.; Lee, J.; Adegoke, O.; Deo, V. K.; Abe, F.; Suzuki, T.; Park, E. Y. Single-Step Detection of Norovirus Tuning Localized Surface Plasmon Resonance-Induced Optical Signal between Gold Nanoparticles and Quantum Dots. *Biosens. Bioelectron.* **2018**, *122*, 16−24.
(55) Saha, B.; Evers, T. H.; Prins, M. W. J. How Antibody Surface Coverage on Nanoparticles Determines the Activity and Kinetics of Antigen Capturing for Biosensing. *Anal. Chem.* **2014**, *86*, 8158.
(56) Oliveira, J. P.; Prado, A. R.; Keijok, W. J.; Antunes, P. W. P.; Yapuchura, E. R.; Guimarães, M. C. C. Impact of Conjugation Strategies for Targeting of Antibodies in Gold Nanoparticles for Ultrasensitive Detection of 17$\beta$-Estradiol. *Sci. Rep.* **2019**, *9*, 13859.
(57) Fu, X.; Wang, Y.; Liu, Y.; Liu, H.; Fu, L.; Wen, J.; Li, J.; Wei, P.; Chen, L. A Graphene Oxide/Gold Nanoparticle-Based Amplification Method for SERS Immunoassay of Cardiac Troponin I. *Analyst* **2019**, *144*, 1582−1589.
(58) Zhang, C.; Wang, C.; Xiao, R.; Tang, L.; Huang, J.; Wu, D.; Liu, S.; Wang, Y.; Zhang, D.; Wang, S.; Chen, X. Sensitive and Specific Detection of Clinical Bacteria: Via Vancomycin-Modified $Fe_3O_4$@Au Nanoparticles and Aptamer-Functionalized SERS Tags. *J. Mater. Chem. B* **2018**, *6*, 3751−3761.
(59) Chen, J.; Li, Y.; Huang, K.; Wang, P.; He, L.; Carter, K. R.; Nugen, S. R. Nanoimprinted Patterned Pillar Substrates for Surface-Enhanced Raman Scattering Applications. *ACS Appl. Mater. Interfaces* **2015**, *7*, 22106.
(60) Puppulin, L.; Hosogi, S.; Sun, H.; Matsuo, K.; Inui, T.; Kumamoto, Y.; Suzaki, T.; Tanaka, H.; Marunaka, Y. Bioconjugation Strategy for Cell Surface Labelling with Gold Nanostructures Designed for Highly Localized PH Measurement. *Nat. Commun.* **2018**, *9*, 5278.
(61) Sánchez-Purrà, M.; Roig-Solvas, B.; Rodriguez-Quijada, C.; Leonardo, B. M.; Hamad-Schifferli, K. Reporter Selection for Nanotags in Multiplexed Surface Enhanced Raman Spectroscopy Assays. *ACS Omega* **2018**, *3*, 10733−10742.


https://dx.doi.org/10.1021/acsami.0c14729
*ACS Appl. Mater. Interfaces* XXXX, XXX, XXX−XXX